

Article

Thin-Film Composite Membranes with a Carbon Nanotube Interlayer for Organic Solvent Nanofiltration

Mingjia Liao¹, Yun Zhu², Genghao Gong^{3,*}  and Lei Qiao^{4,*}

¹ Chemical Engineering Department, Chongqing Chemical Industry Vocational College, Chongqing 401228, China

² Institute of Resources and Security, Chongqing Vocational Institute of Engineering, Chongqing 401228, China

³ State Key Laboratory of Separation Membranes and Membrane Processes, School of Materials Science and Engineering, Tiangong University, Tianjin 300387, China

⁴ Chongqing Academy of Eco-environmental Sciences, Chongqing 401147, China

* Correspondence: gonghaog@hotmail.com (G.G.); cqulqiao@163.com (L.Q.)

Abstract: Compared to the traditional chemical-crosslinking-based polymer, the porous polytetrafluoroethylene (PTFE) substrate is considered to be an excellent support for the fabrication of thin-film composite (TFC) organic solvent nanofiltration (OSN) membranes. However, the low surface energy and chemical inertness of PTFE membranes presented major challenges for fabricating a polyamide active layer on its surface via interfacial polymerization (IP). In this study, a triple-layered TFC OSN membrane was fabricated via IP, which consisted of a PA top layer on a carbon nanotube (CNT) interlayer covering the macroporous PTFE substrate. The defect-free formation and cross-linking degree of the PA layer can be improved by controlling the CNT deposition amount to achieve a good OSN performance. This new TFC OSN membrane exhibited a high dye rejection (the rejection of Bright blue B > 97%) and a moderate and stable methanol permeated flux of approximately 8.0 L m⁻² h⁻¹ bar⁻¹. Moreover, this TFC OSN membrane also exhibited an excellent solvent resistance to various organic solvents and long-term stability during a continuous OSN process.



Citation: Liao, M.; Zhu, Y.; Gong, G.; Qiao, L. Thin-Film Composite Membranes with a Carbon Nanotube Interlayer for Organic Solvent Nanofiltration. *Membranes* **2022**, *12*, 817. <https://doi.org/10.3390/membranes12080817>

Academic Editor: Zhiwei Qiao

Received: 10 August 2022

Accepted: 18 August 2022

Published: 22 August 2022

Publisher's Note: MDPI stays neutral with regard to jurisdictional claims in published maps and institutional affiliations.



Copyright: © 2022 by the authors. Licensee MDPI, Basel, Switzerland. This article is an open access article distributed under the terms and conditions of the Creative Commons Attribution (CC BY) license (<https://creativecommons.org/licenses/by/4.0/>).

Keywords: polytetrafluoroethylene; carbon nanotube interlayer; polyamide; thin-film composite membrane; organic solvent nanofiltration

1. Introduction

With the development of the industrial technology, a variety of organic solvents such as alkanes, lipids, ketones and alcohols are widely used in organic synthesis, separation and catalyst recycling [1]. The pollution problem caused by the widespread use of organic solvents has become increasingly prominent, which seriously threatens the environment and health of the human body. Traditional techniques for separating, retrieving and purifying organic solvents are mainly distillation and extraction. However, these traditional separation technologies typically present disadvantages such as the large footprint and high energy consumption. Organic solvent nanofiltration (OSN), as a new type of pressure-driven membrane separation technology [2,3], has progressively attracted more attention from researchers because of its environment-friendly characteristics, high separation efficiency and low energy consumption [4]. The OSN technique can efficiently separate molecules of 200–1000Da from various organic solvents and has great potential for catalyst and solvent recovery and purification of active pharmaceutical ingredients [5–8].

Currently, the integrally skinned asymmetric and thin-film composite (TFC) membranes prepared via phase inversion and interfacial polymerization (IP), respectively, are two typical OSN membrane types. Compared to the phase inversion method, TFC OSN membranes prepared by IP can separately adjust the microstructure and thickness of the skin layer and the porous substrate, thereby significantly improving their permselectivity. The state-of-the-art TFC membrane consists of a polyamide (PA) separation layer and a

porous support [9]. The former plays a key role in the separation performance of membranes, whereas the latter generally acts as a mechanical support. Therefore, the separation performance of TFC PA membranes can be adjusted by adjusting the microstructure and surface property of the PA top layer. In recent decades, the vast majority of studies focused on regulating the structure of the PA layer to enhance the permselectivity of TFC membranes by controlling the IP conditions, such as diffusion rates and concentrations of monomers, time and temperature of the IP process and types and concentrations of additives [10–12]. In addition to these, the post-treatment of PA networks and surface modification of the substrate in the IP reaction also significantly influenced the formation and performance of the PA layer for TFC membranes.

Recently, for example, Solomon and co-workers performed interfacial polymerization on a cross-linked polyimide substrate to prepare a new TFC PA membrane that can be applied to the separation of organic solvent systems, such as DMF, THF, methanol and toluene [13]. After immersing the prepared TFC membrane in DMF, a small amount of PA without crosslinking dissolved, thus enhancing the microporosity of the PA. Hence, the permeation flux of the TFC membrane greatly improved without destroying the structure of the PA layer. Livingston and co-workers deposited cadmium hydroxide nanostrands onto a UF membrane support to prepare an ultrathin PA layer via IP. This TFC membrane exhibited a high organic solvent permeation flux due to its ultrathin thickness of 10 nm [14]. Meanwhile, Gong and co-workers fabricated a PA active layer onto an intermediate layer consisting of carbon nanotubes (CNT) that was covered on a polyethersulfone microfiltration membrane [15]. The presence of this CNT interlayer with a smooth surface facilitates the construction of the dense and thin PA top layer. This TFC PA membrane exhibited a high divalent salt rejection (>98.3%) and dye rejection (>99.5%) with a high pure water flux of around $21 \text{ L m}^{-2} \text{ h}^{-1} \text{ bar}^{-1}$. Moreover, CNT interlayers were prepared on various substrates including PAN nanofiber and PES microfiltration membranes via spray coating [16] and Inkjet printing [17] methods, respectively, and the as-prepared TFC membranes have been applied to the FO [18] and NF, confirming an improved water permeance and antifouling performance [19,20]. These results indicated that the presence of an intermediate layer could effectively decrease the thickness of PA membranes via the avoidance of the intrusion of PA into the porous substrate.

On the other hand, OSN membranes generally require insoluble in organic solvents or only have a small degree of swelling because of their harsh application environments [21]. Compared with the commercialized porous polymeric substrates such as polysulfone and polyethersulfone, polytetrafluoroethylene (PTFE) has many unique merits including excellent thermal stability, acid and alkali tolerance and solvent resistance [22]. However, owing to their insoluble characteristic in organic solvents, most of the porous PTFE membranes were usually prepared via mechanical biaxial stretching, spinning or auxiliary-assistant pore forming methods, resulting in a rough surface and large pore size (0.5–5 μm) of these PTFE membranes [23], which was unfavorable for preparing the PA layer via the IP method. Moreover, the low surface energy and chemical inertness of PTFE membranes also presented major challenges while using the IP method to prepare the PA top layer on the PTFE surface, besides a poor adhesion on the interface between the PA and PTFE layer [24,25].

In this work, therefore, we constructed a polydopamine-modified carbon nanotube (PDA-CNT) firstly, followed by depositing the PDA-CNT onto a porous PTFE substrate as an interlayer. After that, an ultrathin PA active layer was fabricated on top of the PDA-CNT interlayer via IP. PDA, as a modifier or coating material, has been widely used in preparation and surface modification of various solvent-resistant membranes due to its good solvent stability and high adhesion to most materials [26]. Therefore, this thin PDA-CNT interlayer acts as a bridging layer linking the PA top layer with the PTFE substrate, thereby improving the structural stability of this triple-layered TFC OSN membrane. Meanwhile, we investigated the impact of the PDA-CNT interlayers on the formation of the PA top layer by adjusting the structure and property of the PDA-CNT

interlayer. Finally, a high-performance TFC OSN membrane was fabricated via IP, which exhibited a great promise for applications in the organic solvent nanofiltration process.

2. Experimental Section

2.1. Materials

PTFE microfiltration membranes with a pore size about $0.25\mu\text{m}$ were obtained from Hangzhou Yibo Separation Membrane Co., LTD. (Hangzhou, China). Single-walled carbon nanotubes (CNTs, diameter $< 2\text{ nm}$, length: $5\text{--}30\ \mu\text{m}$, purity: $>95\%$) were purchased from XFNANO (Nanjing, China). Sodium dodecylbenzenesulfonate (SDS), methyl orange (99%), methyl violet (99%), acid magenta (99%), congo red (99%) and bright blue B (99%) were purchased from Sahn Chemical Technology Co., Ltd. (Shanghai, China). Benzoyl chloride (TMC) was obtained from Beijing Bellingway Technology Co., Ltd. (Beijing, China). M-phenylenediamine (MPD) was obtained from Sigma Aldrich (St. Louis, MA, USA). Tris-HCl solution (0.1 mol/L , $\text{pH} = 7.5$) was obtained from Beijing Lambost Biotechnology Co., Ltd. (Beijing, China). Dopamine hydrochloride (99%) was obtained from J&K Chemical Co., Ltd. (Hangzhou, China). N-hexane, Methanol, Anhydrous ethanol and N, N-dimethyl were purchased from Tianjin Kemiou Chemical Reagent Co., Ltd. (Tianjin, China).

2.2. Fabrication of the TFC OSN Membrane

Polydopamine-modified CNT (PDA-CNT) dispersion was prepared by following the reported procedure [27]. Briefly, CNT (10 mg) and SDS (100 mg) were added to DI water (100 mL) and then sonicated at 270 W for 10 h, followed by centrifuge at 10,000 rpm for 1 h to remove undispersed CNT. Subsequently, dopamine hydrochloride (10 mg) and 0.1 m HCl-Tris solution (10 mL, $\text{pH} = 7.5$) were added into the CNT dispersion, the mixed solution was stirred for more than 12 h at $40\ ^\circ\text{C}$. Finally, the homogeneous PDA-CNT dispersion was obtained after 30 min centrifugation at 10,000 rpm.

The CNT interlayer was fabricated by the vacuum filtration method. Briefly, the CNT layer was made by filtering a certain amount of PDA-CNT dispersion onto the porous PTFE substrate (deposition area: 0.0016 m^2) under a constant pressure of 1 bar using a vacuum pump on the permeate side, as shown in Figure 1. Hence, the deposition amount of CNT layer can be controlled by the filtration volume of the CNT dispersion. After that, the PTFE-CNT composite membrane was placed in the oven to dry at $40\ ^\circ\text{C}$. Subsequently, the polyamide (PA) active layer was fabricated on the surface of PTFE-CNT membrane at room temperature. First, the PTFE-CNT substrate was fixed on surface of a plate and clamped with a PTFE frame, then dipped in 5.0 wt% MPD aqueous solution for 2 min. Excess MPD solution on the substrate surface was removed with a rubber roller. Then, 0.2 wt% TMC/hexane solution was poured onto the whole top surface of the composite membrane for 30 s at room temperature and an active PA layer was formed. After washing the membrane with pure hexane, the resulting membranes were cured at $65\ ^\circ\text{C}$ for 10 min. Finally, the obtained PTFE-CNT-PA (named TFC) membrane was stored in DI water at $4\ ^\circ\text{C}$ for further use and characterization.

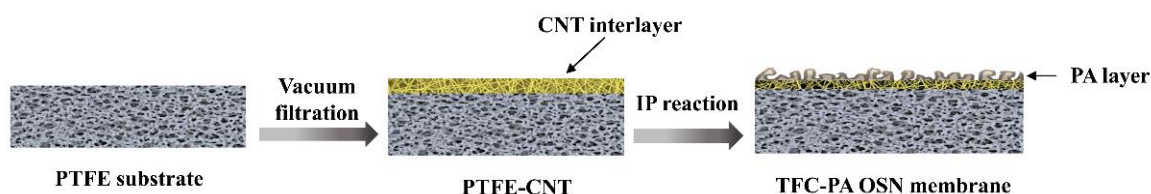


Figure 1. Schematic illustration of the preparation process of PTFE-CNT-PA membrane.

2.3. Characterization

All samples were dried for 4 h in a vacuum chamber before characterization. The structures and morphologies of the membrane were measured by field emission scanning electron microscopy (SEM) (Hitachi, S-4800, Tokyo, Japan) with an acceleration voltage of 10 kV. The surface topography of the membrane was characterized using an atom force

microscopy (AFM, Bruker, Dimension Icon, Karlsruhe, Germany) under a tapping mode at atmospheric condition. The elemental composition of the PA layer was analyzed by an X-ray photoelectron spectrometer (XPS, Thermofisher, ESCALAB 250Xi, Waltham, MA, USA). Water contact angles of membrane surfaces were detected using a contact angle meter (DSA20, Krüss, Hamburg, Germany) at room temperature. The pore size of membranes was detected by bubble point method using a pore size analyzer (3H-2000 PB, Beijing, China).

2.4. OSN Performance Test

The solvent flux and dye rejection experiments of TFC OSN membranes were carried out using a simple device with a dead-end permeation cell (effective membrane area of 2.8 cm²), as shown in Figure 2. The TFC OSN membrane was precompact with corresponding pure solvent at 7 bar and 25 °C for 1 h to achieve a steady permeation flux before the filtration experiments. Dye concentration of feed solution was 20 ppm and the physicochemical properties of the dyes used are summarized in Table 1. The concentrations of various dye solutions in the feed and permeated sides were measured using a UV-vis spectrometer (UV2700, Shimadzu, Kyoto, Japan). All the OSN tests were performed at 25 °C with a pressure of 6 bar. The solvent flux (J) and permeance (P) of the OSN membrane can be calculated by Formulas (1) and (2):

$$J = \frac{m}{\rho \times S \times t} \quad (1)$$

$$P = \frac{J}{\Delta p} \quad (2)$$

where: J is the permeation flux of the solution (L m⁻² h⁻¹), m is the mass of the permeate solution (g), ρ is the density of the solvent (g/L), S is the effective membrane area (m²), Δp is the test pressure (bar) and t is the test time (h). The dye rejection (R) of membranes was calculated by the following Equation (3):

$$R = \left(1 - \frac{C_p}{C_f}\right) \times 100\% \quad (3)$$

where C_p and C_f are dye concentration of the permeated and feed side, respectively. In all experiments, at least three specimens for each data point were tested and the results are reported as the average of the measured values with standard deviation as error bars.

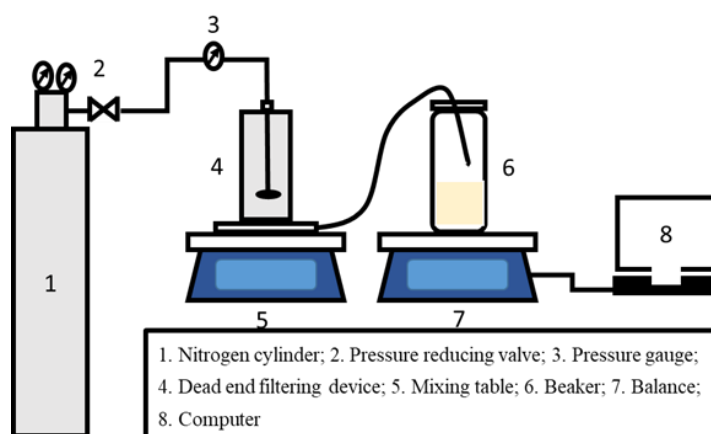


Figure 2. Schematic drawing of the lab-scale dead-end organic solvent nanofiltration (OSN) system.

Table 1. The information of dyes used in this work.

Dye Type	Charge	Molecular Weight (Da)	Molecular Size (nm × nm)
Methyl orange	-	327	1.13 × 0.42
Methyl violet	-	394	1.44 × 1.45
Acid magenta	-	588	1.1 × 1.2
Congo red	-	697	2.56 × 0.73
Bright blue B	-	826	2.06 × 1.79

3. Results and Discussion

3.1. Structure and Properties of PDA-CNT Interlayer on the PTFE Substrate

The polydopamine (PDA)-modified carbon nanotube (CNT) interlayer was deposited on a porous PTFE substrate using the vacuum filtration of PDA-CNT dispersion. The effect of PDA-CNT deposition on the surface morphology and properties of the PTFE substrate was studied, since it would directly influence the formation of the polyamide (PA) active layer via interfacial polymerization (IP), and thus affect the separation performance of the TFC OSN membrane. Figure 3 shows the SEM and AFM images of the structure and morphology of the PDA-CNT interlayer prepared with different filtration volumes of PDA-CNT dispersion on PTFE substrates. Meanwhile, the surface roughness (R_a) and average pore size of PTFE-CNT gradually decreased from 70 to 27.3 nm and 261.5 to 47.7 nm, respectively, with an increase in the CNT deposition amount, as shown in Table 2. These results indicated that a smoother and denser CNT interlayer could be formed on the PTFE substrate with an increased CNT deposition amount. In addition, compared to original PTFE substrate, the PTFE-CNT membrane decreased the water contact angles from 100.9 to 43.1° (Table 2), indicating a more hydrophilic surface due to the presence of the hydrophilic PDA-coated CNT layer, which is beneficial to the subsequent IP process to form the PA active layer. These results forcefully demonstrate that the PDA-CNT interlayer obviously changed the surface property and morphology of the porous PTFE substrate, including the reduction of pore size, roughness and water contact angle of the substrate.

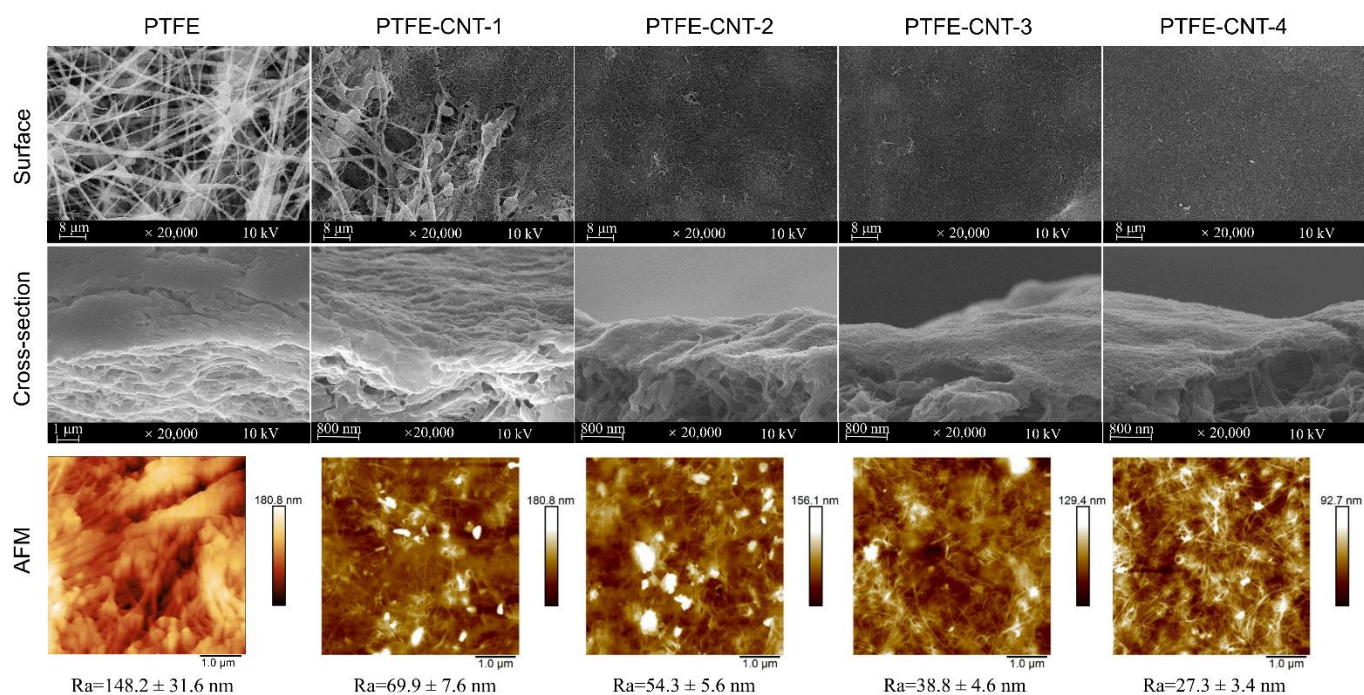


Figure 3. Surface and cross-sectional SEM images of the PTFE-CNT membranes as well as their corresponding surface AFM images.

Table 2. Structure and properties of the Pristine PTFE and the PTFE-CNT Membrane.

Samples	CNT Dispersion Volume (mL)	Surface Roughness (nm)	Average Pore Size (nm)	Water Contact Angle (°)
PTFE	0	148.2 ± 36.1	261.5	100.9 ± 3.7
PTFE-CNT-1	1	69.9 ± 7.6	146.4	81.3 ± 4.9
PTFE-CNT-2	2	54.3 ± 5.6	69.9	63.7 ± 3.1
PTFE-CNT-3	3	38.8 ± 4.6	51.66	42.6 ± 2.2
PTFE-CNT-4	4	27.3 ± 3.4	47.7	43.1 ± 1.9

3.2. Effect of CNT Interlayer on the Formation of PA Active Layer

The PA active layer was prepared on the PTFE-CNT substrate with different CNT deposition amounts (0~4 mL) via the IP reaction of MPD and TMC. The PTFE-CNT-PA composite membranes were named TFC-PA (without CNT layer) and TFC-PA-1~4, referring to the filtrated volume of CNT dispersion from 1 to 2, 3 and 4 mL. Figure 4 shows the SEM and AFM images of structure and morphology of the TFC-PA membranes prepared under different filtration volumes of CNT dispersion. It was obvious that at a low CNT deposition amount (0 and 1 mL), the surface of the prepared TFC-PA membrane had leaf-like structures with a high surface roughness. With an increase in the CNT deposition amount, the leaf-like structure of the PA surface gradually changed into a typical “nodular” feature, thus to form a more uniform and smoother surface (top line in Figure 4). This was probably because the hydrophilic PDA-CNT interlayer could store diamine solution and retard the IP reaction, which restrained the formation of big leaf-like structures on the PA surface, thereby leading to the formation of a smoother PA surface with small nodular structures. This is consistent with the changes of surface roughness of TFC PA membranes from the AFM images (bottom line).

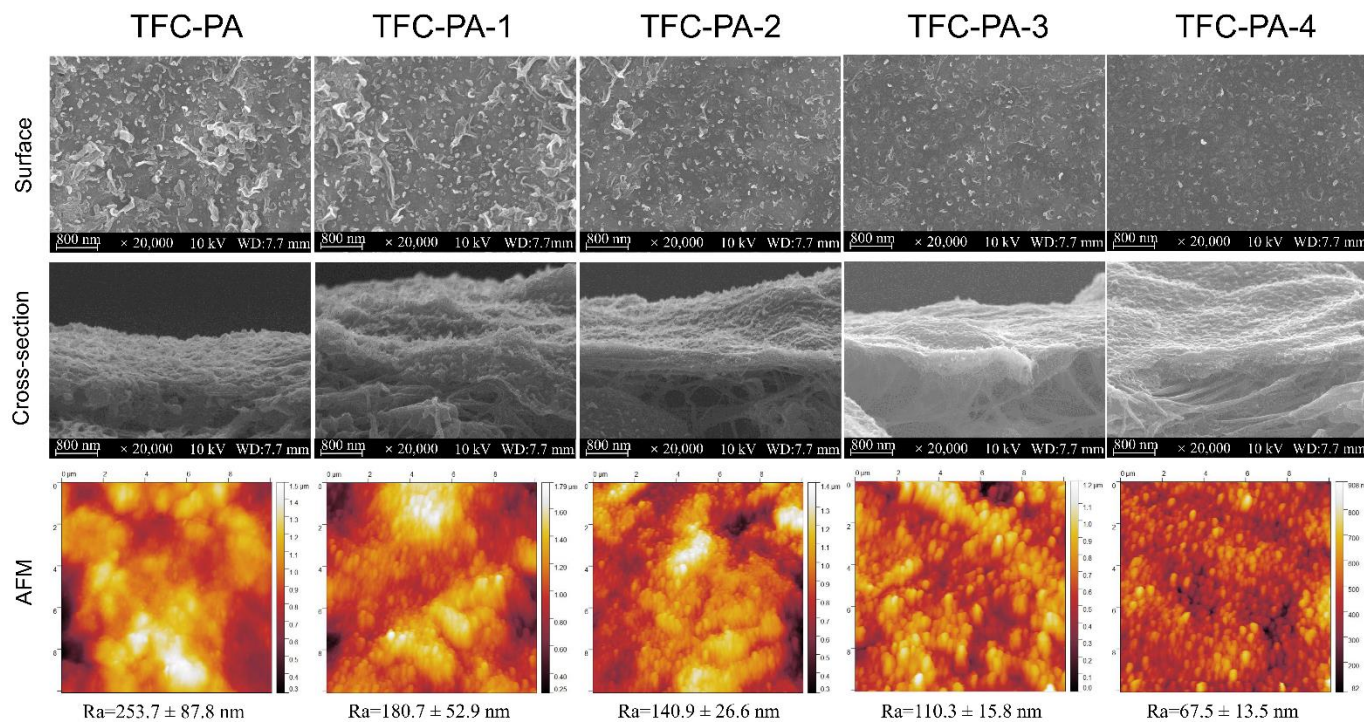


Figure 4. Surface and cross-sectional SEM images of the TFC-PA membranes with different CNT amounts, as well as their corresponding surface AFM images (TFC-PA-1~4 refer to the filtrated volume of CNT dispersion from 1 to 2, 3 and 4 mL).

Owing to the ultrathin CNT layer and rough PTFE surface, it was difficult to observe and distinguish triple-layered TFC PA from the cross-sectional SEM images of TFC membranes in Figure 4 (middle line). Therefore, the PA layer was further investigated using XPS. Table 3 showed the elemental compositions and degree of cross-linking of PA layers from TFC-PA membranes prepared with different CNT deposition amounts. It was found that the cross-linking degree of the PA layer gradually increased (TFC-PA-1~3) and then decreased (TFC-PA-4) with an increasing CNT dispersion amount. This was because the presence of the CNT interlayer decreased the roughness of the membrane surface, causing a more even distribution of the MPD and TMC monomers during IP, resulting in higher degrees of cross-linkage (TFC-PA-1~3) [28]. Meanwhile, the packing density of the CNT interlayer gradually increased with the increase of the CNT deposition amount, the produced heat from the IP reaction between MPD and TMC was difficult to dissipate in the denser CNT networks with smaller pore size, leading to instantaneously rising temperatures in the interface, thus further intensifying the IP reaction [29]. However, it can be found that when the CNT deposition amount increases from 3 to 4 mL, the cross-linking degree of the PA layer decreased from 54 (TFC PA-3) to 29% (TFC PA-4). This was also probably because the thicker and denser hydrophilic CNT layer can store more diamine solution, which suppress the diamine monomer molecule toward the oil phase and retards the IP reaction in a short time, resulting in the formation of a PA layer with a low cross-linking degree and surface roughness [30]. The same results were shown in Figure 5. Figure 5 showed the O1s core-level spectra of the synthesized TFC PA membranes. The O1s core-level spectrum of PA can be curve-fitted into two peak components of carbonyl oxygen (O=C-N) with binding energy at 531.0 eV and carboxylic oxygen (O=C-O) with binding energy at 532.5 eV. These results also showed that the degree of the PA surface cross-linking gradually increased and then decreased with an increase in the CNT deposition amount. It was concluded that the TFC PA-3 membrane exhibited the highest cross-linking degree, which is beneficial to improve the selectivity of the TFC OSN membrane.

Table 3. Elemental compositions of PA layers from TFC-PA membranes (the degree of cross-linking of PA active layer was calculated from the ratio of network to linear cross-linked portion of the polymer).

Samples	CNT Amount (mL)	C1s (%)	O1s (%)	N1s (%)	O/N Ratio $\left[\frac{O}{N} = \frac{3X+4Y}{3X+2Y} \right]$	Degree of Network Cross-Linking (%) $\left[DNC = \frac{X}{X+Y} \times 100\% \right]$
Fully cross-linked (Y = 0)	-	75.00	12.50	12.50	1.00	100%
Fully linear (X = 0)	-	71.40	19.10	9.50	2.00	0%
TFC PA-1	1.0	70.07	16.23	10.38	1.56	34%
TFC PA-2	2.0	71.58	15.22	10.18	1.50	40%
TFC PA-3	3.0	70.99	13.60	9.98	1.36	54%
TFC PA-4	4.0	70.26	16.37	10.09	1.62	29%

3.3. OSN Performance of the Fabricated TFC-PA Membranes

The OSN performance of the TFC PA OSN membranes for methyl orange/methanol (MO/MeOH) solution was evaluated using a dead-end membrane cell, and the results are shown in Figure 6. The TFC PA-0 (PTFE-PA) membrane showed a high MeOH flux and a quite low MO rejection of around 12.0%. This might be because the rough surface and large pore size of the PTFE substrate with a low surface energy was adverse to fabricate the PA layer via the IP process, resulting in the defect formation of the PA top layer on its surface, as mentioned previously. Nevertheless, compared to the TFC PA-0 membrane, TFC PA-1 with a CNT interlayer showed a reduced MeOH flux and a significant rise in MO rejection, which increased from 12.0 to 77.4%. This indicated that the presence of a CNT interlayer on PTFE substrates could significantly improve the PA formation via the IP method. Moreover, MeOH flux was gradually reduced while the MO rejection further increased with increases

in the CNT deposition amount (TFC PA-1~3). This was because the cross-linking degree of the PA top layers gradually increased with an increase in the CNT deposition amount (Table 3 and Figure 5), leading to the formation of a denser PA layer, thereby improving the MO rejection. Compared to the TFC PA-3 membrane, however, TFC PA-4 with a higher CNT deposition amount presented a relatively low MO rejection. This was caused by a reduced cross-linking degree of the PA top layer of the TFC PA-4 membrane. As a result, the TFC PA-3 membrane exhibited a moderate permeate flux of $7.8 \text{ L m}^{-2} \text{ h}^{-1} \text{ bar}^{-1}$ and the highest MO rejection of 91.5%.

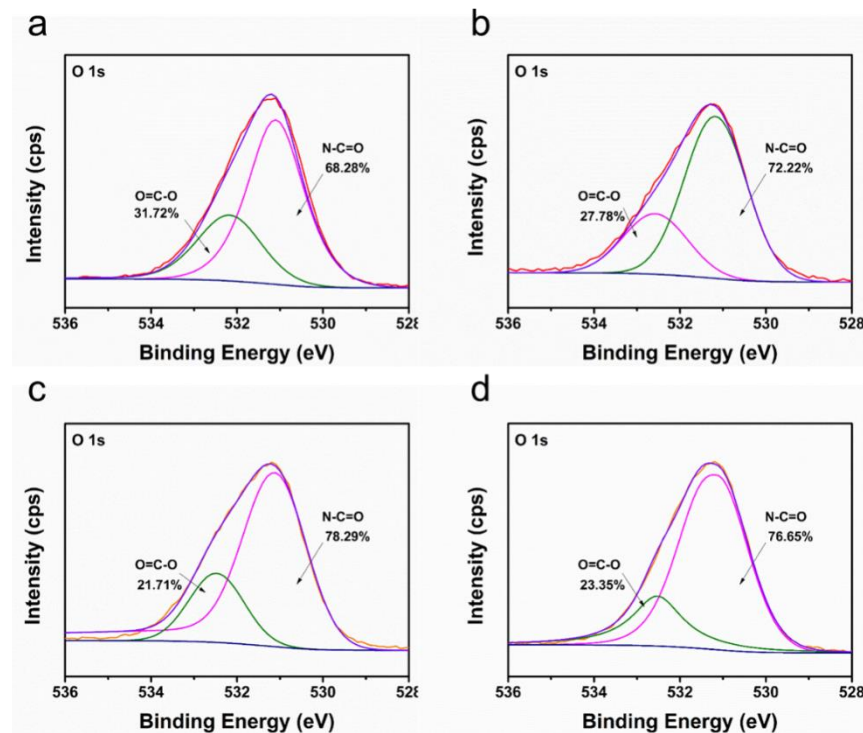


Figure 5. XPS O1s spectra of TFC-PA membranes prepared with different CNT deposition amounts ((a–d) corresponding to TFC PA-1~4 membranes).

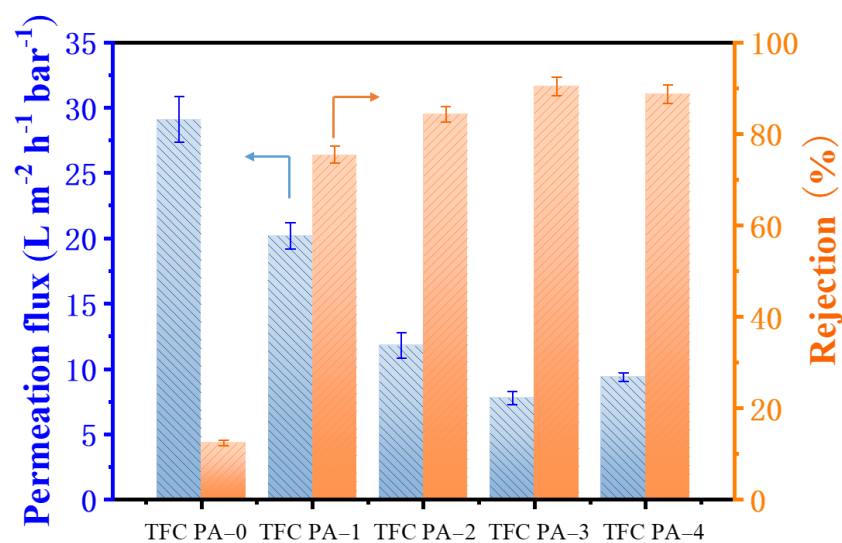


Figure 6. Permeate flux and dye rejection of the TFC OSN membranes with different CNT deposition amounts for the methyl orange/methanol solution (The arrow points to the corresponding Y-axis).

Figure 7 exhibited the correlation between organic solvent properties (including viscosity, molar diameter and solubility parameter) and permeance of the TFC PA-3 membrane. It presented a linear relationship between the solvent property and permeance (Figure 7b). Moreover, acetonitrile and methanol exhibited relatively high permeance due to their high solubility parameter (polar component) and low viscosity and molecular diameter. In contrast, owing to relatively high viscosity and molar diameter, as well as low solubility parameters, propanol and ethanol showed relatively low permeance. These results indicated that the solubility parameter and viscosity of the solvent apparently influence permeance of the TFC PA OSN membranes. As a result, for those organic solvents with similar molecular size, a solvent with low viscosity and high affinity for the polar PA membrane exhibits a relatively high permeation flux. Moreover, this TFC PA OSN membrane with the triple-layered structure also showed an excellent stability in various organic solvents.

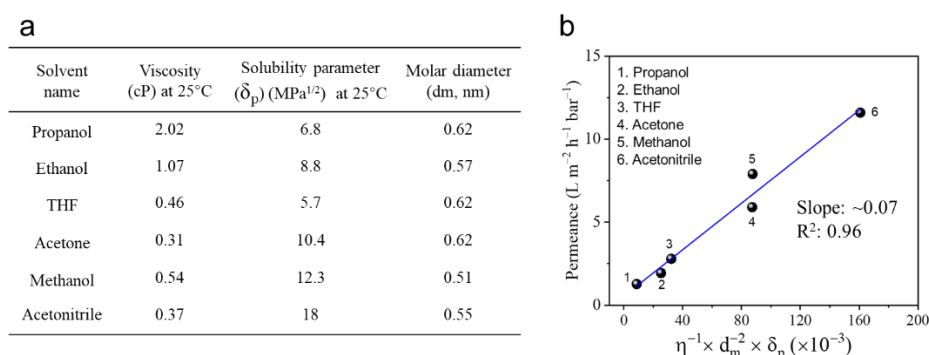


Figure 7. (a) Properties of solvents used in this work and their (b) correlation with solvent permeance of TFC PA-3 membranes (one membrane for every single data point).

To further explore the OSN performance of the TFC PA membrane, a series of dyes/MeOH solutions with different molecular weights were examined as feed solution for OSN tests and the results are presented in Figure 8. The TFC PA-3 membrane showed high dye rejections for Bright blue B (97.7%), Congo red (94.8%), Acid Fuchsin (93.5%), Methyl violet (92.9%) and Methyl orange (91.5%). Although the dye rejection slightly decreased with a reduction of the molecular weight of dyes, this TFC PA exhibited a stable methanol permeate flux of approximately $7.9 \text{ L m}^{-2} \text{ h}^{-1} \text{ bar}^{-1}$. Moreover, according to the rejection values of these dyes, the molecular weight cut-off of the TFC PA membrane is about 320 Da. These results suggested that the presence of this CNT interlayer facilitates the high-quality fabrication of the dense and thin PA top layer on macroporous PTFE substrates via IP method.

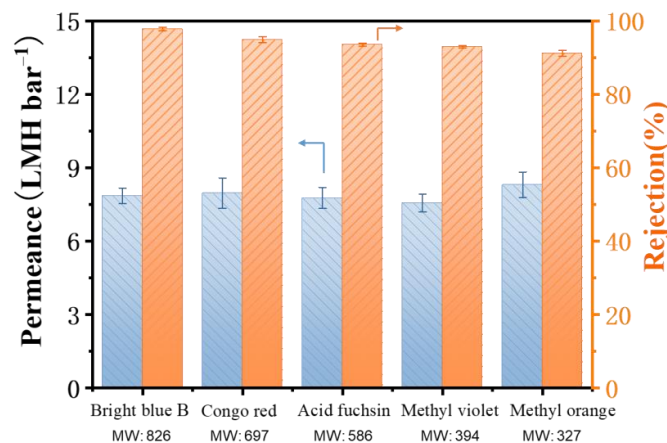


Figure 8. The permeance and rejection of the TFC PA-3 OSN membrane with various dyes/methanol solutions (one membrane for every single data point and the arrow points to the corresponding Y-axis).

Figure 9 shows the long-term time course for OSN performance of the TFC PA-3 membrane for filtrating 20 ppm Methyl orange/MeOH solution. This triple-layered TFC PA membrane exhibited a high Methyl orange rejection (~92%) and constant methanol flux of approximately $8.0 \text{ L m}^{-2} \text{ h}^{-1} \text{ bar}^{-1}$ after 24h continuous OSN test. This result showed that the triple-layered TFC PA membrane had an excellent long-term stability and OSN performance compared to the OSN performance of the other OSN membranes reported previously (Table 4).

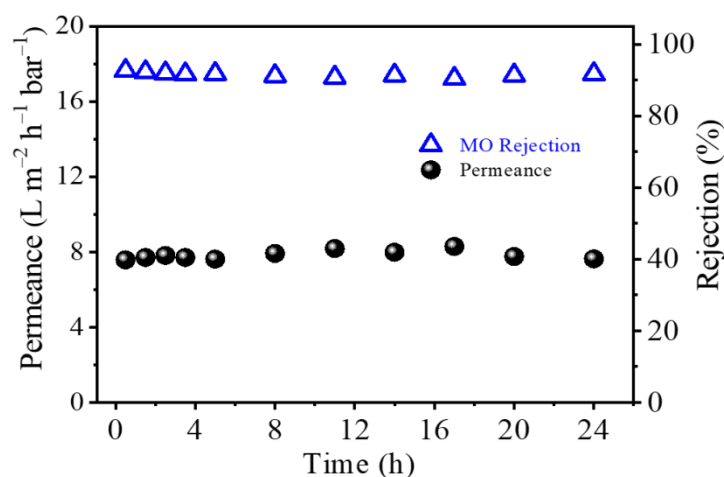


Figure 9. Long-term performance of the TFC PA-3 membrane for the separation of a 20 ppm MO/MeOH solution at 6 bar and 25 °C (one membrane coupon for all measures).

Table 4. Comparison of the performance of our TFC PA OSN membrane with other TFC PA OSN membranes reported in the literature.

Membrane	Substrate	Solvent/Dye (MW)	Permeance (LMH/Bar)	Rejection (%)	Ref.
PA	Ceramic substrate	Methanol/Methyl orange (327)	26.3	30.6	[31]
	Polypropylene	Methanol/Brilliant blue R (826)	1.5	88	[32]
	Matrimid [®] 5218	Methanol/Tetracycline (444)	5.1	95	[33]
	XP84	Methanol/Styrene oligomers (400)	1.5	98	[34]
	Matrimid [®] polyimide dual layer	Methanol/Ramazol brilliant blue (626.5)	0.9	99.3	[35]
	PSF-SPESS	Methanol/Bromothymol blue (624)	2.4	92	[36]
PA/MOFs	Crosslinked Matrimid [®] 5218	Methanol/Tetracycline (444)	20	99	[37]
	P84	Methanol/Styrene oligomers (236)	4.2	96	[38]
PA	PTFE	Methanol/ Methyl orange (327)	7.9	92	This work

4. Conclusions

A triple-layered TFC OSN membrane that was comprised of a PA top layer, a PDA-CNT interlayer and a macroporous PTFE substrate was successfully fabricated via the IP method. The deposition quality and cross-linking degree of the PA layer can be improved by adjusting the CNT deposition amount, thus to achieve a good OSN performance. This new TFC OSN membrane showed a high dye rejection (the rejection of Bright blue B > 97%) and a moderate and stable methanol permeated flux of approximately $8.0 \text{ L m}^{-2} \text{ h}^{-1} \text{ bar}^{-1}$. Moreover, this TFC OSN membrane also exhibited an excellent solvent resistance to various organic solvents and long-term stability during a continuous OSN process, suggesting the macroporous PTFE substrate can be an excellent support instead of the traditional chemical-crosslinking-based polymer supports for the fabrication of TFC PA OSN membranes.

Author Contributions: Conceptualization, L.Q. and G.G.; methodology, M.L.; software, L.Q.; validation, Y.Z. and L.Q.; formal analysis, Y.Z.; investigation, M.L.; resources, M.L.; data curation, M.L. and G.G.; writing—original draft preparation, M.L.; writing—review and editing, G.G.; visualization, L.Q.; supervision, L.Q. and G.G.; project administration, M.L.; funding acquisition, M.L. All authors have read and agreed to the published version of the manuscript.

Funding: This study was supported by the project of science and technology research program of Chongqing Education Commission of China. (No. KJQN201904501) and Natural Science Foundation of Chongqing, China (cstc2020jcyj-msxmX0989).

Institutional Review Board Statement: Not applicable.

Informed Consent Statement: Not applicable.

Data Availability Statement: The outcomes of this study have been included within the text.

Acknowledgments: The authors are grateful for the Researchers Supporting science and technology research program project from the Chongqing Education Commission of China. (No. KJQN201904501) and the Science and Technology Plans of Tianjin (No. 20ZYJDC00100).

Conflicts of Interest: The authors declare no conflict of interest.

References

1. Marchetti, P.; Jimenez Solomon, M.F.; Szekely, G.; Livingston, A.G. Molecular separation with organic solvent nanofiltration: A critical review. *Chem. Rev.* **2014**, *114*, 10735–10806. [[CrossRef](#)]
2. Namvar-Mahboub, M.; Pakizeh, M. Optimization of preparation conditions of polyamide thin film composite membrane for organic solvent nanofiltration. *Korean J. Chem. Eng.* **2014**, *31*, 327–337. [[CrossRef](#)]
3. Wu, C.; Liu, S.; Wang, Z.; Zhang, J.; Wang, X.; Lu, X.; Jia, Y.; Hung, W.S.; Lee, K.R. Nanofiltration membranes with dually charged composite layer exhibiting super-high multivalent-salt rejection. *J. Membr. Sci.* **2016**, *517*, 64–72. [[CrossRef](#)]
4. Vandezande, P.; Gevers, L.E.; Vankelecom, I.F. Solvent resistant nanofiltration: Separating on a molecular level. *Chem. Soc. Rev.* **2008**, *37*, 365–405. [[CrossRef](#)]
5. Lin, C.T.; Livingston, A.G. Nanofiltration membrane cascade for continuous solvent exchange. *Chem. Eng. Sci.* **2007**, *62*, 2728–2736. [[CrossRef](#)]
6. Thompson, K.A.; Mathias, R.; Kim, D.; Kim, J.; Rangnekar, N.; Johnson, J.R.; Hoy, S.J.; Bechis, I.; Tarzia, A.; Jelfs, K.E. N-Aryl-linked spirocyclic polymers for membrane separations of complex hydrocarbon mixtures. *Science* **2020**, *369*, 310–315. [[CrossRef](#)]
7. Goh, K.S.; Chen, Y.; Chong, J.Y.; Bae, T.H.; Wang, R. Thin film composite hollow fibre membrane for pharmaceutical concentration and solvent recovery. *J. Membr. Sci.* **2021**, *621*, 119008. [[CrossRef](#)]
8. Shui, X.; Li, J.; Zhang, M.; Fang, C.; Zhu, L. Tailoring ultrathin microporous polyamide films with rapid solvent transport by molecular layer-by-layer deposition. *J. Membr. Sci.* **2021**, *628*, 119249. [[CrossRef](#)]
9. Khorshidi, B.; Thundat, T.; Fleck, B.A.; Sadzadeh, M. A Novel Approach Toward Fabrication of High Performance Thin Film Composite Polyamide Membranes. *Sci. Rep.* **2016**, *6*, 22069. [[CrossRef](#)]
10. Ghosh, A.K.; Jeong, B.H.; Huang, X.F.; Hoek, E.M.V. Impacts of Reaction and Curing Conditions on Polyamide Composite Reverse Osmosis Membrane Properties. *J. Membr. Sci.* **2008**, *311*, 34–45. [[CrossRef](#)]
11. Klaysom, C.; Hermans, S.; Gahlaut, A.; Van Craenenbroeck, S.; Vankelecom, I.F.J. Polyamide/Polyacrylonitrile (PA/PAN) Thin Film Composite Osmosis Membranes: Film Optimization, Characterization and Performance Evaluation. *J. Membr. Sci.* **2013**, *445*, 25–33. [[CrossRef](#)]

12. Khorshidi, B.; Thundat, T.; Fleck, B.A.; Sadrzadeh, M. Thin Film Composite Polyamide Membranes: Parametric Study on the Influence of Synthesis Conditions. *RSC Adv.* **2015**, *5*, 54985–54997. [[CrossRef](#)]
13. Solomon, J.; Fernanda, M. Thin Film Composite Membranes by Interfacial Polymerization for Organic Solvent Nanofiltration. Ph.D. Thesis, Imperial College London, London, UK, 2013.
14. Karan, S.; Jiang, Z.; Livingston, A.G. Sub-10 nm polyamide nanofilms with ultrafast solvent transport for molecular separation. *Science* **2015**, *348*, 1347. [[CrossRef](#)]
15. Gong, G.H.; Wang, P.; Zhou, Z.Y.; Hu, Y.X. New Insights into the Role of an Interlayer for the Fabrication of Highly Selective and Permeable Thin-Film Composite Nanofiltration Membrane. *ACS Appl. Mater. Interfaces* **2019**, *11*, 7349–7356. [[CrossRef](#)]
16. Yang, Y.; Xu, Y.L.; Liu, Z.J.; Huang, H.Y.; Fan, X.F.; Wang, Y.; Song, Y.X.; Song, C.W. Preparation and characterization of high-performance electrospun forward osmosis membrane by introducing a carbon nanotube interlayer. *J. Membr. Sci.* **2020**, *616*, 118563. [[CrossRef](#)]
17. Park, M.J.; Wang, C.; Seo, D.H.; Gonzales, R.R.; Matsuyama, H.; Shon, H.K. Inkjet printed single walled carbon nanotube as an interlayer for high performance thin film composite nanofiltration membrane. *J. Membr. Sci.* **2021**, *620*, 118901. [[CrossRef](#)]
18. Zhou, Z.Y.; Hu, Y.X.; Boo, C.H.; Liu, Z.Y.; Li, J.Q.; Deng, L.Y.; An, X.C. High-Performance Thin-Film Composite Membrane with an Ultrathin Spray-Coated Carbon Nanotube Interlayer. *Environ. Sci. Technol. Lett.* **2018**, *5*, 243–248. [[CrossRef](#)]
19. Wu, M.B.; Lv, Y.; Yang, H.C.; Liu, L.F.; Zhang, X.; Xu, Z.K. Thin film composite membranes combining carbon nanotube intermediate layer and microfiltration support for high nanofiltration performances. *J. Membr. Sci.* **2016**, *515*, 238–244. [[CrossRef](#)]
20. Long, L.; Wu, C.Y.; Yang, Z.; Tang, C.Y.Y. Carbon Nanotube Interlayer Enhances Water Permeance and Antifouling Performance of Nanofiltration Membranes: Mechanisms and Experimental Evidence. *Environ. Sci. Technol.* **2022**, *56*, 2656–2664. [[CrossRef](#)]
21. Valtcheva, B.I.; Kumbharkar, C.S.; Kim, F.J.; Bhole, Y.; Livingston, A.G. Beyond polyimide: Crosslinked polybenzimidazole membranes for organic solvent nanofiltration (OSN) in harsh environments. *J. Membr. Sci.* **2014**, *457*, 62–72. [[CrossRef](#)]
22. Briguori, C.; Sarais, C.; Colombo, A. The polytetrafluoroethylene-covered stent: A device with multiple potential advantages. *Int. J. Cardiovasc. Interv.* **2009**, *4*, 145–149. [[CrossRef](#)] [[PubMed](#)]
23. Feng, S.S.; Zhong, Z.X.; Wang, Y.; Xing, W.H.; Drioli, E. Progress and perspectives in PTFE membrane: Preparation, modification, and applications. *J. Membr. Sci.* **2018**, *549*, 332–349. [[CrossRef](#)]
24. Mortazavi, M.; Fazeli, A.; Moghaddam, S. Scalable Bonding of Nanofibrous Polytetrafluoroethylene (PTFE) Membranes on Microstructures. *J. Micromech. Microeng.* **2018**, *28*, 015001. [[CrossRef](#)]
25. Jin, X.; Strueben, J.; Heepe, L.; Kovalev, A.; Mishra, Y.K.; Adelung, R.; Gorb, S.N.; Staubitz, A. Joining the Un-Joinable: Adhesion Between Low Surface Energy Polymers Using Tetrapodal ZnO Linkers. *Adv. Mater.* **2012**, *24*, 5676–5680. [[CrossRef](#)]
26. Zhang, C.; Lv, Y.; Qiu, W.; He, A.; Xu, Z.K. Polydopamine Coatings with Nanopores for Versatile Molecular Separation. *ACS Appl. Mater. Interfaces* **2017**, *9*, 14437–14444. [[CrossRef](#)] [[PubMed](#)]
27. Zhu, Y.Z.; Xie, W.; Gao, S.J.; Zhang, F.; Zhang, W.B.; Liu, Z.Y.; Jin, J. Single-Walled Carbon Nanotube Film Supported Nanofiltration Membrane with a Nearly 10 nm Thick Polyamide Selective Layer for High-Flux and High-Rejection Desalination. *Small* **2016**, *12*, 5034–5041. [[CrossRef](#)]
28. Gonzales, R.R.; Zhang, L.; Guan, K.C.; Park, M.J.; Phuntsho, S.; Wahab, A.A.; Matsuyama, H.; Shon, H.K. Aliphatic polyketone-based thin film composite membrane with mussel-inspired polydopamine intermediate layer for high performance osmotic power generation. *Desalination* **2021**, *516*, 115222. [[CrossRef](#)]
29. Ma, X.H.; Yao, Z.K.; Yang, Z.; Guo, H.; Xu, Z.L.; Tang, C.Y.Y.; Elimelech, M. Nanofoaming of Polyamide Desalination Membranes to Tune Permeability and Selectivity. *Environ. Sci. Technol. Lett.* **2018**, *5*, 123–130. [[CrossRef](#)]
30. Wang, J.J.; Yang, H.C.; Wu, M.B.; Zhang, X.; Xu, Z.K. Nanofiltration Membranes with Cellulose Nanocrystals as an Interlayer for Unprecedented Performance. *J. Mater. Chem. A* **2017**, *5*, 16289. [[CrossRef](#)]
31. Xia, L.; Ren, J.; Weyd, M.; McCutcheon, J.R. Ceramic-supported thin film composite membrane for organic solvent nanofiltration. *J. Membr. Sci.* **2018**, *563*, 857–863. [[CrossRef](#)]
32. Kosaraju, P.B.; Sirkar, K.K. Interfacially polymerized thin film composite membranes on microporous polypropylene supports for solvent-resistant nanofiltration. *J. Membr. Sci.* **2008**, *321*, 155–161. [[CrossRef](#)]
33. Sun, S.-P.; Chung, T.-S.; Lu, K.-J.; Chan, S.-Y. Enhancement of flux and solvent stability of Matrimid® thin-film composite membranes for organic solvent nanofiltration. *AIChE J.* **2014**, *60*, 3623–3633. [[CrossRef](#)]
34. Jimenez Solomon, M.F.; Bhole, Y.; Livingston, A.G. High flux membranes for organic solvent nanofiltration (OSN)-Interfacial polymerization with solvent activation. *J. Membr. Sci.* **2012**, *423*, 371–382. [[CrossRef](#)]
35. Sun, S.-P.; Chan, S.-Y.; Chung, T.-S. A slow-fast phase separation (SFPS) process to fabricate dual-layer hollow fiber substrates for thin-film composite (TFC) organic solvent nanofiltration (OSN) membranes. *Chem. Eng. Sci.* **2015**, *129*, 232–242. [[CrossRef](#)]
36. Peyravi, M.; Rahimpour, A.; Jahanshahi, M. Thin film composite membranes with modified polysulfone supports for organic solvent nanofiltration. *J. Membr. Sci.* **2012**, *423*, 225–237. [[CrossRef](#)]
37. Guo, X.; Liu, D.; Han, T.; Huang, H.; Yang, Q.; Zhong, C. Preparation of thin film nanocomposite membranes with surface modified MOF for high flux organic solvent nanofiltration. *AIChE J.* **2017**, *63*, 1303–1312. [[CrossRef](#)]
38. Sorribas, S.; Gorgojo, P.; Tellez, C.; Coronas, J.; Livingston, A.G. High flux thin film nanocomposite membranes based on metal-organic frameworks for organic solvent nanofiltration. *J. Am. Chem. Soc.* **2013**, *135*, 15201–15208. [[CrossRef](#)]